

Journal of Materials Chemistry B

Materials for biology and medicine

Accepted Manuscript

This article can be cited before page numbers have been issued, to do this please use: D. Lubrin, C. Elliott, J. Desaulniers and T. Stotesbury, *J. Mater. Chem. B*, 2026, DOI: 10.1039/D5TB02880A.



This is an Accepted Manuscript, which has been through the Royal Society of Chemistry peer review process and has been accepted for publication.

Accepted Manuscripts are published online shortly after acceptance, before technical editing, formatting and proof reading. Using this free service, authors can make their results available to the community, in citable form, before we publish the edited article. We will replace this Accepted Manuscript with the edited and formatted Advance Article as soon as it is available.

You can find more information about Accepted Manuscripts in the [Information for Authors](#).

Please note that technical editing may introduce minor changes to the text and/or graphics, which may alter content. The journal's standard [Terms & Conditions](#) and the [Ethical guidelines](#) still apply. In no event shall the Royal Society of Chemistry be held responsible for any errors or omissions in this Accepted Manuscript or any consequences arising from the use of any information it contains.

1 **Impact of 2'-fluoro nucleobase modifications on CD detection, sensitivity and**
2 **specificity of short oligonucleotides bound to alginate hydrogels**

3 *Daisee K. Lubrin¹, Colin I. Elliott¹, Jean-Paul Desaulniers², Theresa Stotesbury^{2*}.*

4 ¹Applied Bioscience Graduate Program, Faculty of Science, Ontario Tech University,
5 2000 Simcoe St N, Oshawa, Ontario, L1G 0C5, Canada

6 ² Faculty of Science Ontario Tech University, 2000 Simcoe St N, Oshawa, Ontario, L1G
7 0C5, Canada

8 * Email: theresa.stotesbury@ontariotechu.ca
9

10 **KEYWORDS** Biosensor, biomaterial, DNA, RNA, click chemistry, spectral analysis,
11 chemometrics
12
13



14 **Abstract**

15 Chemical modification of oligonucleotides has aided in the advancement of various
16 therapeutic applications; however, their impact on biosensor performance remains
17 understudied. As demand grows for rapid, sensitive, and portable detection technologies
18 in healthcare, environmental, and forensic fields, leveraging the effects of chemical
19 modifications with spectroscopic detection methods offers an opportunity to improve
20 biosensor performance. Herein, we synthesize label-free oligonucleotide-bound alginate
21 hydrogels as biosensors and use circular dichroism (CD) spectroscopy to detect and
22 confirm DNA and RNA hybridization without amplification or labelling. We particularly
23 focus on the impact of 2'-fluoro modifications on biosensor sensitivity and specificity.
24 Fluorine-modified DNA-based biosensors demonstrate more than a threefold increase in
25 sensitivity compared to unmodified DNA. RNA-based biosensors displayed a similar
26 trend, where 2'-fluoro nucleobase modifications significantly lowered the LOD. Biosensor
27 specificity is evaluated by adding mixtures containing up to four non-complementary
28 strands to the alginate-oligo hydrogels. Fluorine-modified biosensors consistently
29 demonstrated greater specificity with more distinct shifts in CD spectra compared to
30 unmodified DNA. Principal component analysis was applied to differentiated samples with
31 and without a bound complement. Additionally, when thermal melt data was combined
32 with CD spectral data it was possible with a random forest model to predict whether
33 unknown samples demonstrated complement binding, with accuracies of 95 % and 83%
34 for 2'-F modified and unmodified oligos, respectively. Our findings highlight the
35 enhancement in biosensor sensitivity and specificity conferred by 2'-fluoro modifications,
36 demonstrating their potential for improved label-free, amplification-free detection of
37 oligonucleotides in complex environmental and forensic samples.

38
39
40
41
42
43
44
45
46



47 1. Introduction

48 Biosensors traditionally consist of a target, a probe/bioreceptor, and a transducer, where
49 the signal transducer converts the bio-recognition event (i.e, binding of probe to the
50 target) into a measurable signal¹. Biosensor design can vary, where the probe could be
51 cells, enzymes, aptamers, or nucleic acids, with responses most often transduced and
52 recorded via optical, electrochemical, or acoustic means¹⁻³. Low analyte concentrations
53 and complex sample matrices are often encountered, leading to increased demand for
54 sensitive, specific, and selective biosensors⁴. Oligonucleotides, particularly DNA, have
55 attractive properties for hydrogel and biosensor synthesis, such as biocompatibility,
56 specific base-pairing, programmability, tunability, and high thermal stability⁵. Hydrogels
57 are three-dimensional cross-linked structures with high water content that can be
58 synthesized using various synthetic and natural polymers⁶⁻⁹. DNA can serve as i) the
59 polymer backbone of the hydrogel, typically formed through self-assembly and
60 hybridization of complementary strands, ii) functionalized cross-linkers, or iii) bioactive
61 molecules rather than structural elements¹⁹. Oligonucleotide-based biosensors are used
62 in various applications, including the sensitive and selective detection of genetic targets,
63 including but not limited to *in vitro* diagnostics and environmental hazard detection^{10,11},
64 clinical diagnostic tests for viral respiratory illnesses^{12,13}, diseases⁷, and the detection of
65 forensically relevant metabolites from seized evidence¹⁴. These biosensors traditionally
66 depend on labelling, amplification, and/or immobilization for detection and signal
67 transduction, which have drawbacks². Labelling approaches, such as the use of
68 molecular beacons, fluorescent tags, fluorophores, or quantum dots, can be challenging,
69 expensive, and time-consuming, while increasing background fluorescence and steric
70 hindrance, reducing the bioaffinity of the probe^{4, 15, 16}. Stimuli-responsive DNA hydrogels
71 are often self-assembled through various amplification techniques, but require
72 complicated steps and produce gels with low mechanical strength¹⁷. Further, amplification
73 of target oligos by polymerase chain reaction (PCR) or isothermal amplification requires
74 multiple sets of specific primers and enzymes¹⁸, which could be prone to off-target effects,
75 primer dimerization, or low amplification efficiency in the presence of inhibitors¹⁹.
76 Electrochemical detection is often used to transduce bio-recognition events, but requires
77 conductive materials, oligo immobilization, and functionalization of electrode and/or
78 sensor surfaces, resulting in complex and costly synthesis¹⁵. The development of a label-
79 free, amplification-free, and immobilization-free oligonucleotide-based biosensor could
80 circumvent these challenges.

81
82 Oligonucleotides can be chemically modified for various applications, altering their
83 structure and function²⁰⁻²⁴, but improving nucleotide stability, binding affinity,
84 pharmacokinetic properties and/or nuclease resistance^{23, 24}. The phosphate backbone,
85 sugar moiety, and nucleobase can all be altered based on the desired application (often
86 therapeutic)^{23, 24}. However, the impact of these chemical modifications on biosensor
87 performance remains largely understudied, prompting us to investigate how these
88 modifications can be harnessed to enhance detection capabilities without the need for
89 labelling, amplification, or immobilization. Fluorine-modified oligonucleotides are of
90 particular interest and contain a fluorine atom at the C2' carbon of the sugar moiety. The
91 high polarity of fluorine attracts the C2' carbon²⁰ of the deoxyribose sugar of the
92 oligonucleotide, causing it to adopt the standard and more stable C3'-endo pucker²⁰,



93 where the 3' carbon bends into the ring, and the bases are oriented further from the helical
94 axis²⁵. The strong electronegativity of fluorine stabilizes the C3'-endo sugar pucker²⁶,
95 creating more polarized nucleobases. This strengthens Watson-Crick base pairing and
96 enhances base stacking^{22, 27}, leading to increased chirality in the molecule. In addition,
97 the 2'-fluoro nucleobase modifications increase nuclease resistance^{28, 29}, affinity to target
98 molecules²⁸, and the stability of the duplex³⁰, which are important considerations in
99 biosensor synthesis. The altered nucleic acid structure and hybridization dynamics could
100 result in more pronounced changes in circular dichroism (CD) spectral signatures. CD is
101 an absorption spectroscopy technique that measures the differential absorption of left and
102 right-circularly polarized light to probe optically active chiral structures. The addition of 2'-
103 fluoro modifications into the oligonucleotide probe of a biosensor could therefore provide
104 a novel, cost-effective way of improving its sensitivity and specificity by capitalizing on
105 these effects.

106
107 In this study, we synthesized and evaluated the performance of short oligonucleotide-
108 bound alginate hydrogels as biosensors, with a particular focus on enhancing sensitivity
109 and specificity through 2'-fluoro nucleobase modifications. Alginate is a negatively
110 charged polysaccharide derived from brown algae and is composed of α -L-guluronic and
111 β -D-mannuronic acid residues³¹. Alginate-based hydrogels exhibit low toxicity, high
112 biocompatibility, and are easily physically and chemically modified³¹. The mechanical,
113 viscoelastic, self-healing, and degradation properties of alginate can be tailored to exhibit
114 various functions³²⁻³⁴. Ionic crosslinking of alginate with divalent cations is the most
115 common method of gelation due to its simplicity and mild reaction conditions³⁵; however,
116 these ionically crosslinked gels lose their mechanical strength over time³⁶. To overcome
117 this loss of mechanical strength, covalently crosslinked hydrogels can be synthesized
118 with crosslinkers³³ such as DNA and RNA. These could further be used as bioinert,
119 biocompatible, biodegradable, and low-cost biosensors with a microstructure resembling
120 the extracellular matrix^{31, 37}. Our biosensor was label-free, amplification-free, and
121 synthesized without a traditional internal signal transducer. Rather, we leveraged the
122 intrinsic chirality and arrangement of nucleobases in oligonucleotides, measuring
123 hybridization to the target oligo with CD spectroscopy³⁸ and exploited the effects of 2'-
124 fluoro nucleobase modifications to enhance biosensor sensitivity and specificity³⁸.

125
126



127 2. Experimental Section

128 2.1 Materials

129 2.1.1 EDC/NHS coupling reaction

130 Alginate sodium salt for brown algae (Sigma; Ontario, Canada), monohydrate free acid
131 (MES) (MP Biomedicals Inc; California, USA), 2-azidoethanamine, sodium hydroxide
132 (Sigma; Ontario, Canada), 1-(3-dimethylaminopropyl)-3-ethylcarbodiimide hydrochloride
133 (EDC) (Tokyo Chemical Industry; Ontario, Canada), N-hydroxysuccinimide (NHS)
134 (Sigma; Ontario, Canada), Amicon Ultra-0.5 Centrifugal Filter Unit (3 kDa MWCO)
135 (Sigma; Ontario, Canada), 11-azido-3,6,9-trioxaundecan-1-amine (Sigma; Ontario,
136 Canada), Amicon Ultra-4 centrifugal filter unit (Sigma; Ontario, Canada), N-
137 hydroxysulfosuccinimide sodium salt (Sulfo-NHS), 97% (Thermo Scientific; Ontario,
138 Canada).

139 140 2.1.2 CuAAC reaction

141 Copper (II) sulfate (Sigma; Ontario, Canada), sodium-L-ascorbate (Sigma; Ontario,
142 Canada), tris(3-hydroxypropyltriazolylmethyl)amine (Sigma; Ontario, Canada),
143 aminoguanidine hydrochloride (Sigma; Ontario, Canada), potassium phosphate
144 monobasic (Thermo Scientific; Ontario, Canada), sodium hydroxide (Sigma; Ontario,
145 Canada).

146 147 2.2 Synthesis of the alginate-azide hydrogel

148 We performed an EDC/NHS coupling reaction adapted from Shi *et al.*³⁹. Briefly, sodium
149 alginate solution (1% w/v) was prepared by dissolving 50 mg (6.68×10^{-2} mM) alginate
150 sodium salt from brown algae in 5 mL of 50 mM (2.50×10^{-1} mM) MES Buffer of pH 5³⁹.
151 The solution was stirred overnight to ensure that it had completely dissolved. 0.116 g of
152 EDC (0.74 mM) and 0.026 g sulfo-NHS (0.12 mM) were added to the alginate dissolved
153 in MES buffer 5 mL and reacted for 30 mins. 28 μ L volume of crosslinker, 2-
154 azidoethanamine (0.33 mM), and 55 μ L of 6 M (1.32 mM) NaOH of pH 8 were
155 subsequently added and left to react at room temperature for 24 hours³⁹. A crosslinker-
156 free control was also synthesized with the same concentrations of reagents, but without
157 the 2'azidoethanamine crosslinker. The Amicon 4K Centrifugal Filter Unit filtered the
158 solution at 12000 rpm for 15 mins at 22°C. Each hydrogel was washed twice with Milli Q
159 water and collected from the filter.

160 2.2.1 Characterization of alginate-azide hydrogel

161

162 2.2.1.1 Fourier-transform infrared spectroscopy (FTIR)

163 A Bruker ALPHA-P compact FTIR spectrometer was used to collect spectra for each of
164 the dried hydrogels. Three drops of each cleaned product were placed in a petri dish (3
165 replicates) and air-dried overnight. Each replicate was scanned on the FTIR spectrometer
166 using the ATR crystal over 400 to 4000 cm^{-1} . Both background scans and sample scans
167 were measured at a resolution of 4 cm^{-1} at 0.75 Hz for a total of 5 scans collected per
168 sample.

169

170 2.2.1.2 Nuclear magnetic resonance (NMR) spectroscopy



171 We acquired ^1H NMR and ^{13}C NMR spectra of the hydrogels using a 400 MHz Bruker
172 IconNMRTM spectrometer. The hydrogels were prepared by drying the cleaned product
173 from 2.2 at 50 °C using a GenevacTM miVac centrifugal concentrator. Dried hydrogels (25
174 – 40 mg) were dissolved in approximately 0.5 mL of D₂O and placed in an NMR glass
175 tube for analysis. 40 and 12500 scans were collected per sample for ^1H NMR and ^{13}C
176 NMR, respectively, at a frequency of 100.67 MHz. ^{13}C NMR spectra were recorded with
177 a sweep width of 24037.73 Hz.

178

179 2.2.1.3 Rheological characterization

180 We diluted (1:4) alginate-azide hydrogel with Milli-Q[®] water to reduce the viscosity of our
181 product and avoid wall slip during rheological measurements. A TA Instruments DHR20
182 stress-controlled rheometer with an advanced Peltier plate and solvent trap system was
183 used to perform an amplitude sweep from 0.01 % to 100 % at a fixed angular frequency
184 of 6.28 rad/s, while frequency sweeps were performed at 22 °C from 0.01 rad/s to 150
185 rad/s at a constant strain amplitude of 0.5 %. Flow sweeps were acquired from 1 - 1200
186 s⁻¹ to measure viscosity.

187

188 2.3. DNA/RNA synthesis

189 Oligonucleotide strands were either **1**) created in our lab using a 394 Applied Biosystems
190 DNA/RNA synthesizer or K&A Synthesizer using standard DNA and RNA
191 phosphoramidites and an alkynyl phosphoramidite from ChemGenes or **2**) purchased
192 from Integrated DNA Technologies (IDT) (Ontario, Canada) (Table 1). Three strands with
193 non-complementary sequences (to the DNA Probe strand) were synthesized or
194 purchased. The Scrambled A strand contained the same nucleotides as the DNA Target
195 strand, but with a randomly scrambled sequence. Scrambled B and Scrambled C have a
196 5' alkyne functionality, and different nucleotide compositions than the DNA Target strand.
197 The mismatched strand is identical to the DNA Target, except for three mismatched
198 nucleotides in the middle of the sequence (Table 1). Two thymine nucleotides were
199 incorporated at the 3' end of the RNA strands.

200

201

202



203 **Table 1:** Sequences of the oligonucleotide strands used in biosensor synthesis. In the
204 mismatch strands, the mismatched nucleotides are bolded and underlined. Thymine
205 nucleotides at the 3' end of RNA strands are designated as "t". 2'-fluorine-modified
206 bases have an "F" subscript.

207
208 † All bases in 2'F Oligo (F-All_{DNA}) and 2'F Oligo (F-All_{RNA}) are 2'F modified except the
209 two thymine bases at the 3' end.
210

Strand	Sequence
DNA Probe	5'-(Alkyne)-ATTCCTGTGTCAGACCCTGtt-3'
DNA Target	5'-CAGGGTCTGACACAGGAAAtt-3'
RNA Probe	5'-(Alkyne)-CUUACGCUGAGUACUUCGAtt-3'
RNA Target	5'-UCGAAGUACUCAGCGUAAGtt-3'
Scrambled A	5'-GGCCTTCACTCGTATGTTATTC-3'
Scrambled B	5'-(Alkyne)-ATTGCGGACTCGATACGATCAT-3'
Scrambled C	5'-(Alkyne)-CAGTCGGTAGTGATATGGCATT-3'
Mismatch (3)	5'-CAGGGTCT <u>GT</u> ACAGAGGAAAtt-3'
Mismatch (5)	5'-CAGGGTCT <u>GT</u> ACAG <u>GATTA</u> AAAtt-3'
Mismatch (7)	5'-CAGG <u>AACGT</u> ACAG <u>GATTA</u> AAAtt-3'
Mismatch (9)	5'-CAGG <u>AACGT</u> ACAG <u>GATTACCT</u> tt-3'
2'-F Oligo (F-3)	5'-(Alkyne)-ATT _F TCCTGTGT _F CAGACCCT _F Gtt-3'
2'-F Oligo (F-6)	5'-(Alkyne)-ATTCCTGT _F G _F T _F C _F A _F G _F ACCCTGtt-3'
2'-F Oligo (F-14)	5'-(Alkyne)-A _F T _F T _F T _F C _F CTGT _F G _F T _F C _F A _F G _F ACCC _F T _F G _F tt-3'
2'-F Oligo (F-All _{DNA})†	5'-(Alkyne)- A _F T _F T _F T _F C _F C _F T _F G _F T _F G _F T _F C _F A _F G _F A _F C _F C _F C _F T _F G _F tt-3'
2'-F Oligo (F-All _{RNA})†	5'-(Alkyne)-C _F U _F U _F A _F C _F G _F C _F U _F G _F A _F G _F U _F A _F C _F U _F C _F G _F A _F tt- 3'

211
212 **2.4 Copper-catalyzed azide-alkyne cycloaddition (CuAAC) reaction**
213 We adapted the copper-catalyzed azide-alkyne cycloaddition (CuAAC) described in
214 Presolski *et al.*⁴⁰. 0.0042 g of alginate-2-azidoethanamine (alginate-azide) hydrogel was
215 dissolved in 114 μL (11.4 nM) of phosphate buffer. 20 nmol of DNA/RNA/2'-F Oligo-Probe
216 strand and 2.5 μL of Solution 1 – 7.5 μL (0.75 nM) of CuSO₄ and 1.5 μL (0.75 nM) of
217 THPTA – were added to the dissolved alginate-azide. 8.33 μL (41.65 nM) of
218 aminoguanidine HCl and 8.33 μL (41.65 nM) of sodium ascorbate were subsequently
219 added. Reagents were allowed to react for 1 hour on a stir plate at 40 °C, then transferred
220 into a 50 kDA MWCO Amicon ultra 0.5 mL centrifugal filter and centrifuged at 12000 rpm
221 at 40 °C for 15 mins. The filter column was washed twice with 300 μL of sterile water and
222 spun again at the same conditions for 15 mins. The filtrate and liquid remaining in the
223 filter were transferred to separate 1.5 mL microcentrifuge tubes. 400 μL of water was
224 added to the small volume (<10 μL) of product remaining in the filter and mixed by
225 pipetting prior to collection.



226
227
228
229
230
231
232
233
234
235
236
237
238
239
240
241
242
243
244
245
246
247
248
249
250
251
252
253
254
255
256
257
258
259
260
261
262
263
264
265
266
267
268
269
270
271

2.4.1 Circular Dichroism (CD) spectroscopy

400 μL of the product from 2.4 was transferred to a 400 μL rectangular quartz cuvette with a 1 mm path length. CD spectra were acquired in triplicate using a Jasco J-815 CD spectropolarimeter at 20 $^{\circ}\text{C}$, recorded every 0.2 nm from 200 to 300 nm at a scanning rate of 100 nm/min. The change in absorbance was measured against a change in CD (mdeg). Samples were automatically baseline-corrected by analyzing the solvent (CD buffer) before each sample measurement. A moving average with a window size of 25 was used to smooth each spectrum.

2.5 Sensitivity and specificity studies

2.5.1 2'-F Modification

The CuAAC reaction described in 2.4 was performed with oligonucleotide sequences containing varying amounts of 2'-fluorine-modified bases (Table 1). For each of these reactions, 20 nmol of the fluorine-modified oligo was covalently bound to the alginate-azide hydrogel. The following 2'-F Oligo sequences were tested: 2'-F Oligo (F-3), 2'-F Oligo (F-6), 2'-F Oligo (F-16), 2'-F Oligo (F-All_{DNA}). CD spectra were acquired to confirm the binding of ss2'-F Oligo to the alginate-azide. An equimolar amount (20 nmol) of the DNA Target was added to the probe-containing alginate-azide hydrogel. The hydrogel was placed in a 94 $^{\circ}\text{C}$ water bath for 2 minutes before cooling at room temperature overnight to ensure annealing. CD spectra were collected for each sample as described in 2.4.1. As a control, identical hybridization experiments were performed using the same 2'-F-modified sequences free in solution without the CuAAC conjugation to alginate. In these experiments, 20 nmol of probe and equimolar target were annealed under the same thermal conditions, and CD spectra were acquired as described in 2.4.1.

2.5.2 Sensitivity Studies

Two different sensitivity studies were performed. In the first, the CuAAC reaction described in 2.4 was repeated with varying amounts of DNA (0 – 83.3) nmol, RNA (0 – 40) nmol, 2'-F Oligo (F-All_{DNA}) (0-20) nmol, and 2'-F Oligo (F-All_{RNA}) (0-20) nmol. CD spectra were first acquired to confirm the binding of single-stranded (ss) DNA/RNA (i.e., Probe strand) to the alginate-azide. An equimolar amount of DNA/RNA complement strand (either 1.25, 2.5, 5, 10, 20, 30, 40, 60 or 83.3) nmol was added to the Probe strand-containing alginate-azide hydrogel. In the second study, the amount of Probe remained constant while the amount of target varied. The CuAAC reaction described in 2.4 was repeated with constant amounts of DNA, RNA, 2'-F Oligo (F-All_{DNA}), and 2'-F Oligo (F-All_{RNA}) (10 nmol). An increasing amount of DNA/RNA Target strand (1.25, 2.5, 5, 10, or 20) nmol was added to the probe-containing alginate-azide hydrogel. In both studies, the hydrogel containing the added complementary strand was placed in a 94 $^{\circ}\text{C}$ water bath for 2 minutes prior to cooling at room temperature overnight to ensure annealing. CD spectra were recorded to confirm complementary binding. Limits of detection (LOD) for the different types of oligo hydrogels were calculated using 3.3 standard deviations of the intercept and the slope of the regression line⁴¹. For comparison to previous literature, the molar LOD amounts were converted to molarity using a volume of 400 μL (volume requirement for CD spectroscopy measurements). The total amount of oligonucleotide added during the click chemistry reaction was used rather than the amount that was

272 successfully conjugated, providing a conservative estimate of sensitivity that accounts for
273 variability in conjugation efficiency.

274

275 2.5.3 Specificity study

276 Combinations of equimolar amounts (i.e., 20 nmol each) of DNA Target, scrambled, and
277 mismatched strands were added to the alginate-ssDNA hydrogel to determine its
278 specificity for its complement (Table 2). CD spectra were collected to assess the binding
279 specificity in each hydrogel. This was repeated with 10 nmol of 2'-F Oligo (F-All_{DNA}) rather
280 than the DNA probe.

281

282 **Table 2.** Types of complement strands added to each hydrogel of the specificity study.
283 Each hydrogel contained the Probe strand (either unmodified DNA or 2'-F Oligo (F-
284 All_{DNA})).

Sample #	DNA Contained in Each Hydrogel
1	No DNA
2	DNA Target Strand
3	Mismatch
4	Mismatch + DNA Target Strand
5	Scrambled A
6	Scrambled A + DNA Target Strand
7	Scrambled B
8	Scrambled B + DNA Target Strand
9	Scrambled C
10	Scrambled C + DNA Target Strand
11	Scrambled B + Scrambled C
12	Scrambled B + Scrambled C + DNA Target Strand
13	Scrambled A + Scrambled B + Scrambled C
14	Scrambled A + Scrambled B + Scrambled C + DNA Target Strand
15	Mismatch + Scrambled A
16	Mismatch + Scrambled A + DNA Target Strand
17	Mismatch + Scrambled A + Scrambled B + Scrambled C
18	Mismatch + Scrambled A + Scrambled B + Scrambled C + DNA Target

285

286

287 2.5.4 Mismatch Determination Threshold Study

288 Combinations of equimolar amounts (i.e., 10 nmol each) of DNA Target, and various
289 mismatched strands were added to the alginate-ssDNA hydrogel to determine the
290 mismatch threshold for discrimination between the perfectly complementary target and
291 sequences containing mismatches (Table 3). CD spectra were collected to assess the
292 binding specificity in each hydrogel.

293

294 **Table 3.** Types of complement strands added to each hydrogel of the mismatch
295 determination threshold study.

Sample #	DNA Contained in Each Hydrogel
1	No DNA Sense
2	DNA Target Strand



296	3	3 Mismatch Sequence	
297	4	3 Mismatch Sequence + DNA Target Strand	
298	5	5 Mismatch Sequence	2.5.5
	6	5 Mismatch Sequence + DNA Target Strand	
	7	7 Mismatch Sequence	
	8	7 Mismatch Sequence + DNA Target Strand	
	9	9 Mismatch Sequence	
	10	9 Mismatch Sequence + DNA Target Strand	

299 *Thermal denaturation studies*

300 Thermal denaturation studies were performed on samples from the specificity study using
 301 a Jasco J-815 CD Spectropolarimeter equipped with a temperature controller. Melting
 302 temperature (T_m) was determined by measuring UV absorbance at 260 nm while the
 303 temperature was increased from 10 to 95 °C at a rate of 0.5 °C per minute. Technical
 304 replicates were conducted by reannealing the strands by placing the sample in a 94 °C
 305 water bath for 2 minutes and then cooling to room temperature overnight. T_m data was
 306 analyzed using Meltwin v3.5 software.

307 *2.5.6 Statistical analyses*

308 Origin Lab software (2024b) was used to plot all spectral data. Peak identification and
 309 maximum absorption wavelength (λ_{max}) were recorded from the ATR-FTIR and CD
 310 spectra. Statistical analyses were completed using R-Studio Software (Version 4.2.2).
 311 Principal component analysis (PCA) was performed on CD spectra obtained from
 312 sensitivity and specificity studies to determine whether hydrogels clustered according to
 313 various physicochemical properties (e.g., type of oligo, conformation, complement
 314 binding, etc). Each spectrum was normalized to its maximum ellipticity value based on
 315 sample type prior to PCA and random forest (RF) computation. RF models were built
 316 with 1000 decision trees and trained with different values of mtry (number of variables to
 317 randomly sample as candidates at each split) and optimized using k-fold ($k = 5$) cross-
 318 validation. The optimized model was then used for predictions. Data was randomly split
 319 into a training and testing set: 4/5 of the data was allocated to the training set, while the
 320 remaining 1/5 made up the testing set. Prediction accuracy was computed by comparing
 321 model classification of test data (i.e., withheld data) with their true classification (i.e., with
 322 or without complement).
 323



3. Results and Discussion

3.1 Binding of Functionalized Oligos to Alginate-azide

327

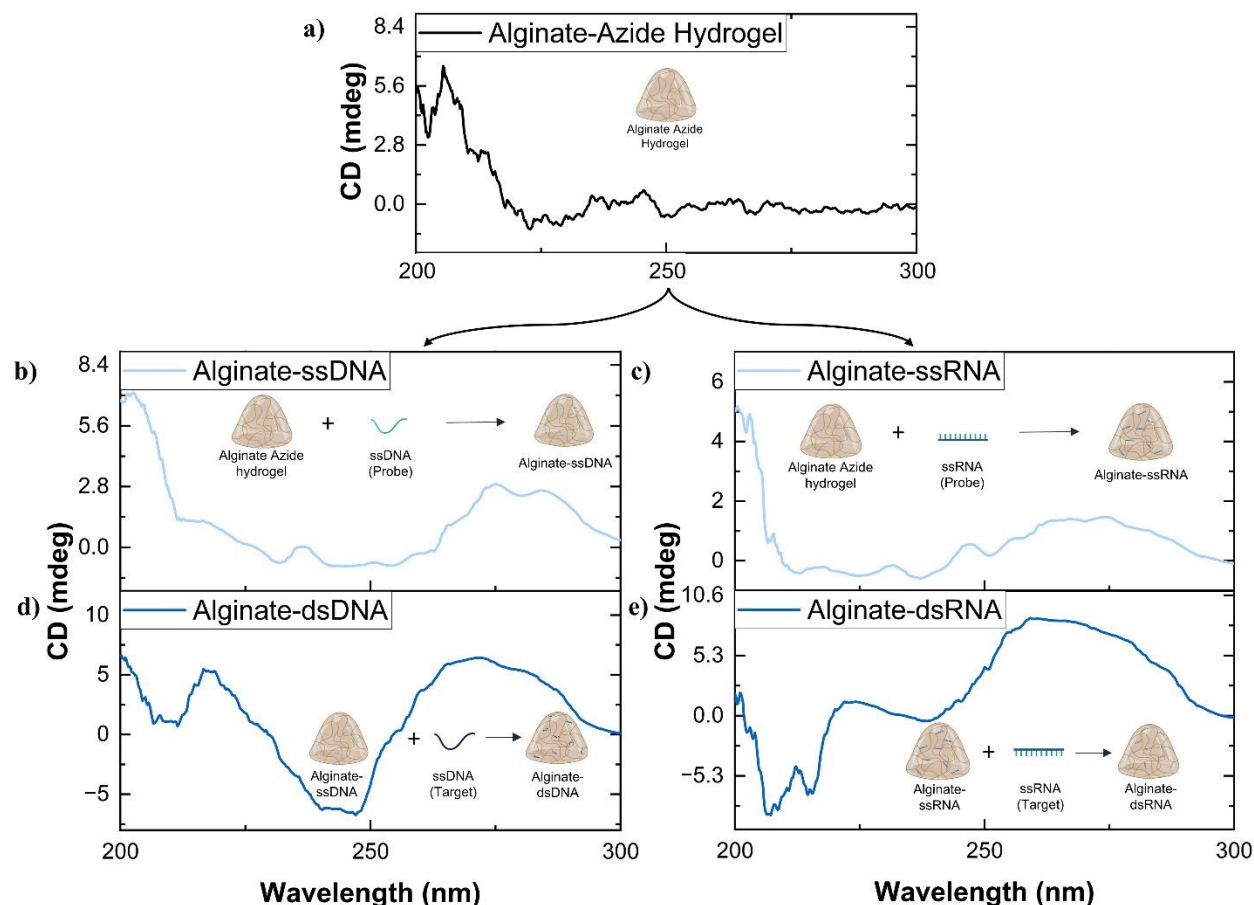
328
329

Figure 1. Example CD spectra from **a)** Alginate-azide, **b)** Alginate-ssDNA, **c)** Alginate-ssRNA, **d)** Alginate-dsDNA, and **e)** Alginate-dsRNA hydrogels collected from the centrifugal filter (i.e., residue). Single-stranded hydrogels contain the Probe strand, while double-stranded (ds) hydrogels include the duplex produced by hybridization of the complementary Target strand.

335

Alginate-oligonucleotide hydrogels were recovered from the filter as residue. The molecular weight of the hydrogel, which comprises the oligonucleotide bound to the alginate-azide backbone, is too large to pass through the centrifugal filter membrane. This format enables effective immobilization of the target sequence and facilitates separation of bound target from unbound or noncomplementary strands. In addition, the hydrogel matrix protects against enzymatic degradation⁴² which may be advantageous for future applications involving sample types where nuclease exposure is expected.

343

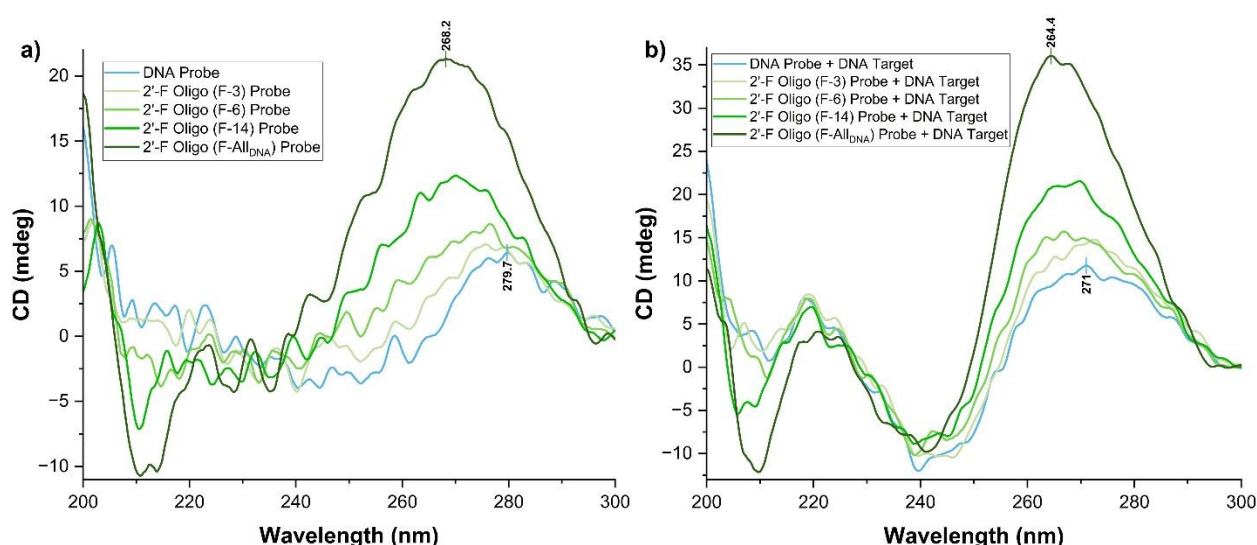
DNA and RNA binding to the alginate-azide hydrogel was confirmed by characteristic changes in CD spectra (Figure 1). Alginate-azide displayed a single peak at ~200 nm and no significant ellipticity bands between 210 nm and 300 nm due to the lack of secondary structure. DNA was successfully bound to the alginate-azide, as observed by the positive

347



348 bands at 220 nm and 260 nm to 280 nm, and a negative band at 245 nm, typical of B-
349 form DNA (Figure 1 b,d)⁴³. These bands displayed larger ellipticity values, blue-shifted
350 maxima, and long-wavelength crossovers upon DNA duplex formation (Figure 1d),
351 indicative of successful hybridization between the target and the probe strand⁴³⁻⁴⁵. RNA
352 was also successfully bound to the alginate-azide as observed by the positive band at
353 260 nm and a negative band at 210 nm (Figure 1c), consistent with the A-form helix of
354 dsRNA^{45, 46}. Both bands had greater ellipticity magnitudes for alginate-dsRNA than
355 alginate-ssRNA, indicating a shift from ssRNA to dsRNA upon hybridization (Figure 1e).
356 Like DNA, RNA could also be detected in the filtrate (Figure S4; filtrate), suggesting that
357 only alginate-azide-bound RNA remained in the filter residue.

3.2 Impact of 2'-Fluorine Modifications on CD Response



361
362 **Figure 2.** CD spectra of a) Probe sequences with an increasing number of 2'-fluoro
363 modified bases bound to alginate and b) the corresponding duplexes with the DNA Target
364 strand as the complement.

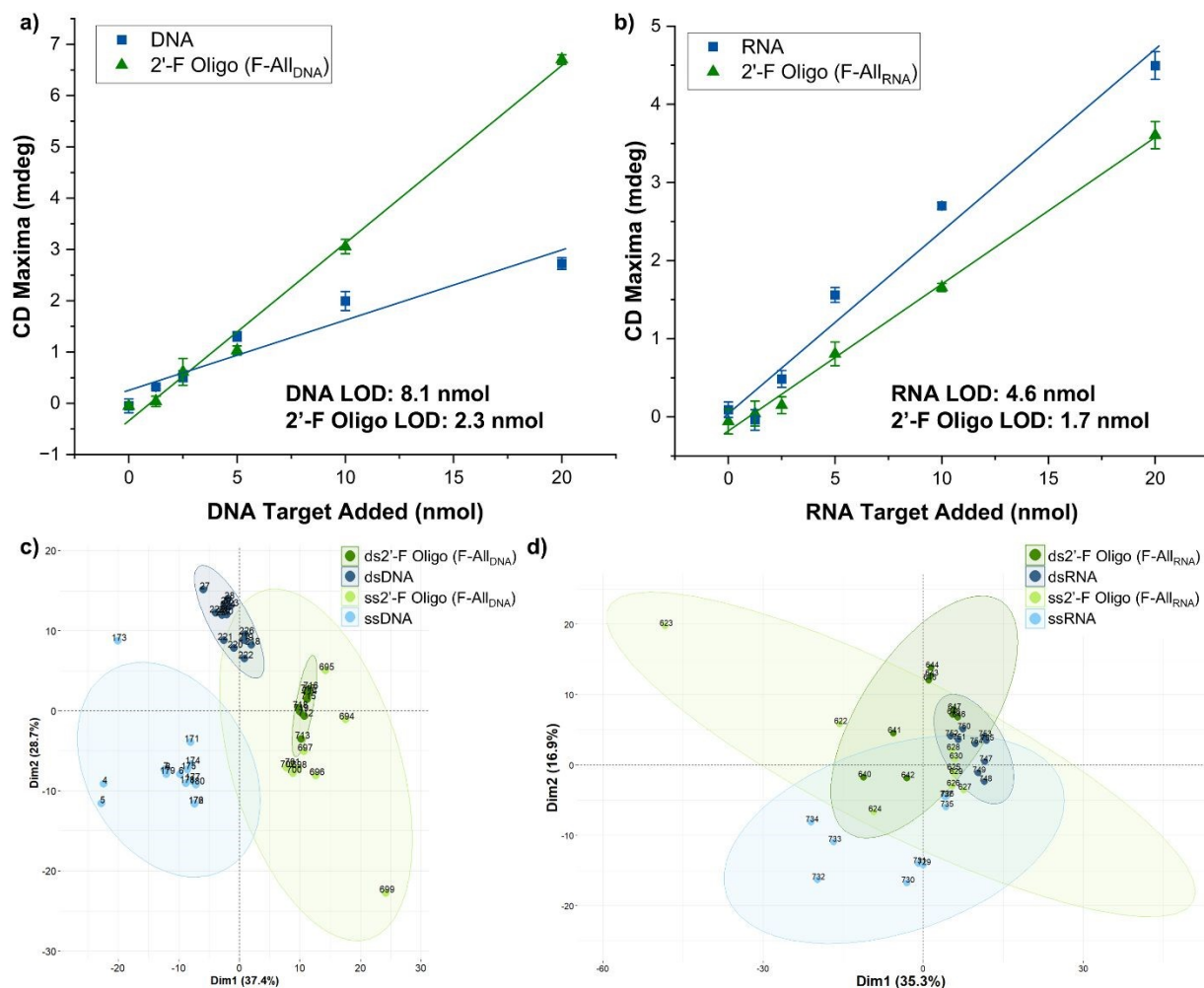
366 The distortion of Watson-Crick base pairs⁴⁷ and nucleobase stacking²⁷ are known to
367 influence CD spectra and are affected by the addition of the highly electronegative fluorine
368 atom. An increase in the number of fluorinated bases in the Probe strand bound to
369 alginate resulted in an increased CD signal intensity and a progressive blue shift in the
370 peak maxima. The unmodified DNA probe displayed the lowest intensity and the most
371 red-shifted peak, while 2'-F Oligo (F-All_{DNA}) displayed the greatest intensity and most
372 blue-shifted peak. As the degree of 2'-F substitution increased, the peak maximum shifted
373 from 279.7 nm to 268.2 nm (Figure 2a). CD response was further enhanced and
374 continued to blue-shift upon hybridization with the complementary unmodified DNA target
375 (Figure 2b), with the peak shifting to 264.4 nm. Notably, the CD signal intensity for the 2'-
376 F Oligo (F-All_{DNA}) + DNA target complex was approximately three times higher than that
377 of the unmodified DNA probe + DNA target complex. Similar results were also observed
378 in the CD signatures of these free probe sequences (not bound to the alginate-azide)
379 (Figure S5). This suggests that oligo modification with fluorine could significantly enhance
380 the sensitivity of our biosensor.



381
382
383
384

3.3. Sensitivity Studies

3.3.1 Sensitivity Study I – Equimolar Amounts of Probe and Target



385

386 **Figure 3.** Calibration curves of **a)** DNA (Slope: 0.136; R^2 : 0.921) and 2'-F Oligo (F-All_{DNA})
 387 (Slope: 0.346; R^2 : 0.993) and **b)** RNA (Slope: 0.233; R^2 : 0.972) and 2'-F Oligo (F-All_{RNA})
 388 (Slope: 0.188; R^2 : 0.996). PCA of ss and ds **c)** DNA and 2'-F Oligo (F-All_{DNA}) and **d)** RNA
 389 and 2'-F Oligo (F-All_{RNA}) for the sensitivity studies with equimolar amounts of probe and
 390 target oligonucleotides added. Ellipses represent the 95 % confidence intervals around
 391 the mean (centroid) of each group. PCAs include samples containing 5-20 nmol of oligo.
 392 PCA samples and their descriptions are included in Table S1.
 393 The average LOD of the alginate-DNA biosensor was 8.1 nmol (20 μ M), while the LOD
 394 for the 2'-F Oligo (F-All_{DNA}) was 2.3 nmol (5.6 μ M), meaning that 2.3 nmol of duplex is
 395 required to obtain an observable signal. Peaks expected of ssDNA and dsDNA begin to
 396 appear at a concentration of 5 nmol and are clearly visible by 10 nmol, while peaks for
 397 ss2'-F Oligo (F-All_{DNA}) and ds2'-F Oligo (F-All_{DNA}) appear at 2.5 nmol and were clearly
 398 visible by 5 nmol, corroborating our computed LOD values (Figure S6 and Figure S8



399 respectively). Similar results were obtained for alginate-RNA hydrogels (Figure S7 and
400 Figure S9), with a LOD of 4.6 nmol (12 μ M) for unmodified RNA and 1.7 nmol (4.6 μ M)
401 for 2'-F Oligo (F-All_{RNA}). 2'-F nucleobase modifications led to a greater increase in the
402 sensitivity of DNA than RNA biosensors. The strong electronegativity of the fluorine atom
403 on the 2' position of the sugar significantly influences sugar puckering, favouring a
404 C3'endo conformation²⁹. This impacts the stability and structure of the duplex⁴⁸, altering
405 base stacking by disrupting the N-glycosidic bond orientation stacking²⁷, resulting in
406 deviations from the classical helical structure. These structural changes are reflected in
407 variations in CD signatures. DNA typically adopts a C2'-endo sugar pucker while RNA
408 naturally assumes a C3'-endo conformation²⁵. The electronegativity of the 2'-fluoro group
409 also more closely resembles that of the 2'-hydroxyl group in RNA than the 2'-hydrogen in
410 DNA. This can be expected to enhance nucleobase polarization, increase Watson-Crick
411 H-bonding strength, and increase enthalpic stabilization due to improved stacking in 2'-F
412 Oligo (F-All_{DNA}) relative to 2'-F Oligo (F-All_{RNA})²⁹. Therefore, fluorine modifications induce
413 more substantial
414 conformational and stacking disruptions in DNA compared to RNA, influencing chirality
415 and, ultimately, biosensor sensitivity. Lower LODs have previously been reported for
416 DNA- and RNA-based biosensors, but those relied on more complex and challenging
417 synthesis and detection techniques, such as immobilization, tagging and/or amplification<sup>2,
418 15, 49</sup>, compared to the simpler label-free, amplification-free approach used in our study.
419



420 Table 4. Comparison of the performance of the proposed biosensor with other reported
421 biosensors for oligonucleotide detection.

Type of Biosensor	Probe/Target	LOD	Benefit	Drawbacks
Electro-chemical ⁵⁰	Probe: DNA on PEG/Ppy nanowire Target: miRNA	0.33 pM	<ul style="list-style-type: none"> Long linear range 	<ul style="list-style-type: none"> Relatively complicated design Requires skilled personnel for operation
Electro-chemical - Differential pulse voltammetry (DVP) ⁵¹	Probe: DNA on MXene w/ Pt/C nanocomposite Target: RNA	0.4 aM	<ul style="list-style-type: none"> 100% accuracy and 97.87% specificity Long linear range 	<ul style="list-style-type: none"> Relatively complicated design
Electro-chemical – Cyclic voltammetry ⁵²	Probe: DNA hairpin with methylene blue and ferrocene Target: DNA	10 pM	<ul style="list-style-type: none"> No bulky equipment needed Not affected by sample's light transmittance 	<ul style="list-style-type: none"> Requires labelling Relatively complicated design Response inversely proportional to [target] 20% loss of signal with washing
Spectral (Fluorescent) ⁵³	Probe: Fluorescein tagged single stranded DNA Target: DNA	15 pM	<ul style="list-style-type: none"> High selectivity (single-mismatch discrimination) Good linear range 	<ul style="list-style-type: none"> Requires PCR amplification Requires skilled personnel for operation
Spectral (Fluorescent) ⁵⁴	Probe: Fluorophore labelled ssDNA Target: DNA	20 pM	<ul style="list-style-type: none"> Multiplex detection of DNA Good dynamic range 	<ul style="list-style-type: none"> Requires amplification Requires skilled personnel for operation
Chiroptical (Our work)	Probe: ssOligo Target: ssOligo	DNA: 9.5 μ M 2'-F Oligo (F All _{DNA}): 7.3 μ M	<ul style="list-style-type: none"> Label-Free Amplification-Free Relatively simple synthesis Relatively low production cost Simple operation 	<ul style="list-style-type: none"> Relatively high LOD



		RNA: 3.2 μM 2'F Oligo (F All_{RNA}): 5.3 μM	<ul style="list-style-type: none"> • Reusable 	
--	--	--	---	--

422
 423 PCA revealed that samples containing unmodified versus 2'F-modified oligos could be
 424 distinguished, highlighting the influence of fluorine modification on CD spectra (Figure
 425 3c). This can be explained due to the natural C2'endo conformation of DNA, which must
 426 now reorganize its conformation to C3'-endo when paired with the 2'-F-modified oligo to
 427 maximize complementary binding thermodynamics. On the other hand, RNA samples
 428 did not cluster as distinctively, and demonstrated some overlap in points and ellipses,
 429 likely due to their preorganized C3'-endo conformation (Figure 3d). Nevertheless, for both
 430 DNA and RNA samples, single-stranded 2'F-oligo probes exhibited greater similarity to
 431 their double-stranded counterparts and clustered closer together than the unmodified
 432 oligonucleotides, likely resulting from the blue shifts in the CD maxima caused by 2'-fluoro
 433 nucleobase modifications. Unmodified ssDNA exhibits a CD maximum at 280 nm
 434 compared to its dsDNA counterpart at 272.6 nm (Figure S6). The introduction of 2'-fluoro
 435 modifications induces significant structural changes, leading to a CD maximum of 265 nm
 436 for both ss 2'-F Oligo (F-All_{DNA}) samples and ds 2'-F Oligo (F-All_{DNA}) samples (Figure S6).
 437 The wavelengths contributing to the highest variance among samples and used to
 438 separate them in the PCA were 259-262 nm and 275-290 nm for dimension 1, and 237-
 439 245 nm for dimensions 2. These represent the regions where the wavebands cross the
 440 x-axis on either side of the positive peak. In unmodified RNA, the ss and ds conformations
 441 have peaks at 272 and 262 nm, respectively, while the fluorine modifications shift the CD
 442 maxima to 264 and 265 nm, respectively (Figure S7). The wavelengths contributing to the
 443 separation of the samples in the PCA were 216-231 nm (i.e., region of the spectra where
 444 the negative peak approaches the x-axis) for dimension 1 and 253-263 nm (i.e., region of
 445 the spectra where the left side of the positive peak approaches the x-axis) for dimension
 446 2. Although data were normalized to the maximum peak intensity, slight tailing persists in
 447 these regions and contributes to the variance detected by the PCA.

448 449 3.3.2 Sensitivity Study II - Constant Probe and Varying Target Sequence



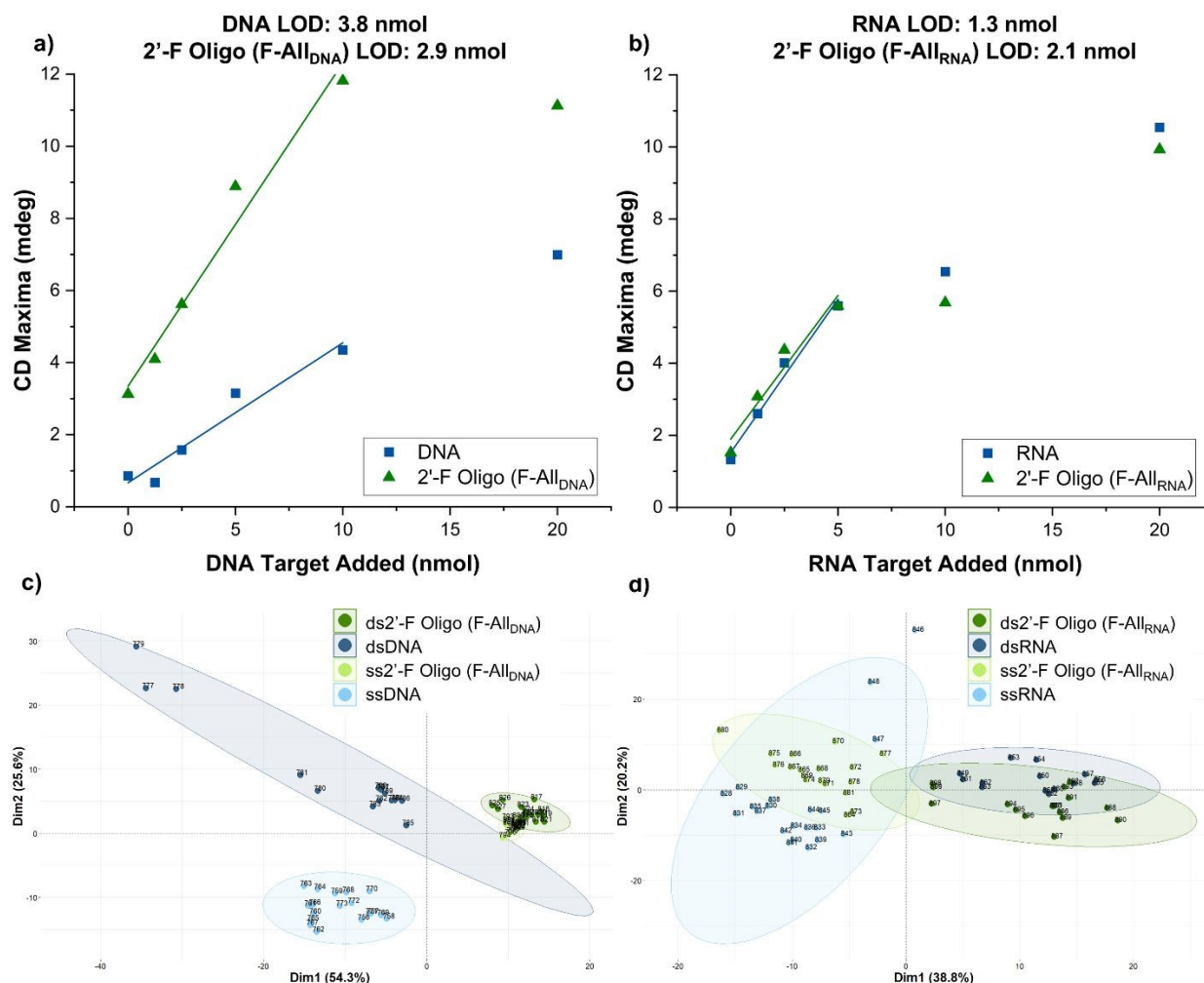


Figure 4. Calibration curves of **a)** DNA (Slope: 0.388; R^2 : 0.939) and 2'-F Oligo (F-All_{DNA}) (Slope: 0.896; R^2 : 0.970) at Positive CD maxima, **b)** RNA (Slope: 0.851; R^2 : 0.980) and 2'-F Oligo (F-All_{RNA}) (Slope: 0.797; R^2 : 0.947) at positive CD maxima. PCA of **c)** ss and ds DNA and 2'-F Oligo (F-All_{DNA}) and **d)** RNA and 2'-F Oligo (F-All_{RNA}) for Sensitivity Studies with constant probe and varying target sequence concentrations. PCAs include all samples containing 1.25-20 nmol of target sequence; CD response from 230-290 nm was used for PCA.

We kept the amount of probe constant at 10 nmol (above the previously determined LOD), while varying the amount of probe from 0 to 20 nmol. Keeping the amount of probe constant while varying the target sequence better simulates real-world scenarios, where the probe and target are likely not present in equimolar amounts. By using data from the positive CD maxima, the LOD was determined to be 3.8 nmol (9.5 μ M) for DNA and 2.9 nmol (7.3 μ M) for 2'-F Oligo (F-All_{DNA}; Figure 4a), indicating that 2.9 nmol of target is required for an observable signal when using 10 nmol of probe. 2'-F Oligo (F-All_{DNA}) exhibited a greater response at the 0 nmol target sequence concentration, representing a scenario where only the single-stranded probe was present (Figure 4a). This elevated response persisted as the target sequence was added, resulting in an overall improved LOD for 2'-F Oligo (F-All_{DNA}). Additionally, the steeper slope observed for the 2'-F Oligo



470 (F-All_{DNA}) calibration curve could be attributed to altered base stacking interactions
471 between the probe and target sequence, which influence the chirality of the molecule and
472 increase the CD response. These findings support the use of 2'-F modifications for
473 enhancing the sensitivity of DNA biosensors. For RNA (Figure 4b), the LOD was 1.3 nmol
474 (3.2 μ M) for unmodified RNA and 2.1 nmol (5.3 μ M) for 2'-F Oligo (F-All_{RNA}). Similar
475 calibration slopes were observed for RNA and 2'-F Oligo (F-All_{RNA}), suggesting that the
476 introduction of the 2'-F modifications does not have a substantial effect on the CD
477 response compared to unmodified RNA, likely due to RNA's preorganized C3'-endo
478 conformation.

479
480 PCA revealed effective clustering, with clear separation between single-stranded and
481 double-stranded unmodified samples (Figure 4c and d). 2'-F modified Oligo clustered
482 tightly and could be distinguished from unmodified DNA samples, indicating greater
483 consistency among samples. Compared to modified RNA, 2'-F modified Oligo exhibited
484 tighter clustering, which could be attributed to its longer linear range and differences in
485 CD maxima, further supporting its use as a biosensor compared to RNA. Unmodified DNA
486 samples with low amounts of the target sequence (specifically the 1.25 nmol sample, 777-
487 779 in the PCA) demonstrated evidence of duplex formation, but were plotted away from
488 the other dsDNA samples (Figure 4c). However, for the 2'-F Oligo (F-All_{DNA}), all samples
489 exhibited a duplex response greater than that of the single-stranded probe, leading to
490 stronger contributions in the PCA. Single-stranded and double-stranded RNA samples
491 clustered together, irrespective of fluorine modification, suggesting minimal effect of the
492 2'-F modifications on CD response, further corroborating the calibration curve in Figure
493 4b. Unmodified and 2'-F Oligos were plotted together for comparative purposes.
494 However, when plotted in separate PCAs, both unmodified and 2'-F modified Oligos had
495 near complete separation based on conformation (i.e., ss vs ds) (Figure S11 and S12).
496 Despite the ss and ds CD maxima of 2'-F Oligos being closer together than their
497 unmodified counterparts, this did not negatively affect target discrimination, and sample
498 types were accurately identified at all target sequence concentrations.

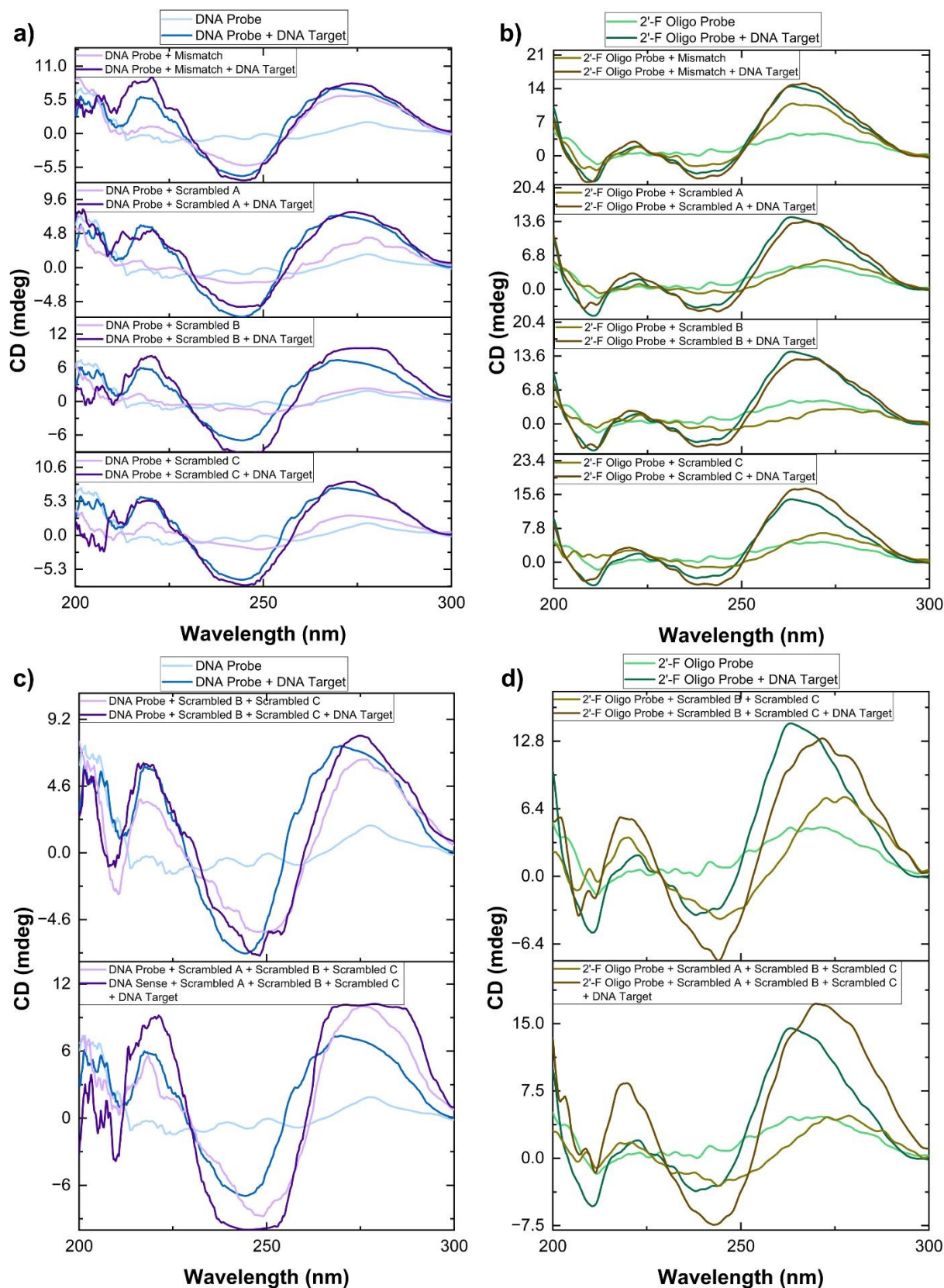
501 3.4 Specificity Study

502
503 Scrambled sequences were introduced in the form of mixtures to evaluate the binding
504 specificity of DNA and 2'-F Oligo probes to the target DNA sequence. In both systems,
505 the addition of scrambled sequences in the absence of the target sequence (Figure 5a,
506 d) produced spectra resembling that of the probe alone in both peak height and location,
507 indicating a lack of binding affinity between the probe and non-complementary
508 sequences. The long wavelength crossover underwent a red shift, contrary to the
509 expected blue shift typically observed during the transition from single- to double-stranded
510 DNA⁴³, with this effect more pronounced in the 2'-F Oligo (F-All_{DNA}) compared to the
511 unmodified DNA. To determine the mismatch discrimination threshold of the DNA probes,
512 additional studies were conducted using target sequences containing 5, 7, and 9
513 mismatches (Figure S13). These results demonstrated that when 5 or more mismatches
514 were present in the target sequence, the corresponding CD spectra could be visually
515 distinguished from samples containing a perfectly complementary target. We then



516 analyzed a sequence with 3 mismatches to evaluate whether the 2'-F oligos displayed
517 enhanced specificity in target binding. Partial binding was observed when a sequence
518 with 3 mismatches was introduced (Figure 5 a and b, top). The resulting spectra were
519 more similar to Figure 5b, top), the peak height for spectra with mismatched sequences
520 (olive green) was between the single-stranded and double-stranded forms. This suggests
521 that hydrogels incorporating 2'-F Oligos potentially offer greater discrimination between
522 mismatched and perfectly complementary target sequences when only 3 bases are non-
523 complementary, compared to those containing unmodified DNA probes. Although
524 discrimination at 3 mismatches is not fully resolved by CD analysis alone, further
525 evaluation using temperature melt analysis (Section 3.4.1) provides additional resolution
526 between perfectly complementary and partially mismatched targets. Together, these
527 results demonstrate robust visual discrimination at ≥ 5 mismatches, while enhanced
528 discrimination at 3 mismatches is achieved when CD and thermal melt analyses are
529 considered in combination.





530
531
532

Figure 5. CD spectra of the DNA hydrogels and 2'-F Oligo hydrogels tested during the specificity study. 2'-F Oligo corresponds to the 2'-F Oligo (F-ALL_{DNA}) sequence. Spectra



533 are compared to Probe strands and a Probe/Target duplex, represented in light blue and
534 dark blue for DNA and light green and dark green for 2'-F Oligo, respectively. CD Spectra
535 in **a)** and **b)** represent samples with a single non-complementary sequence (i.e.,
536 mismatch or scrambled), while spectra in **c)** and **d)** represent samples with multiple non-
537 complementary sequences.

538
539 Subtle differences were observed in CD spectra for larger mixtures containing two or
540 three scrambled sequences with and without the target sequence (**Figure 5c** and **d**). The
541 peak heights of mixtures for unmodified DNA generally resembled those of hydrogels
542 containing the probe-target duplex (**Figure 5c**, light blue). The increased ellipticity near
543 270 nm in hydrogels containing both the probe and multiple scrambled sequences
544 suggests partial duplex formation. Scrambled sequences B and C, containing eight
545 complementary base pairs, might contribute to this elevated ellipticity through partial
546 hybridization with the probe or with each other. However, increased ellipticity could also
547 result from spectral overlap of the ssDNA signal at 280 nm, which would increase if
548 scrambled sequences were retained through encapsulation in the hydrogel. Mixtures with
549 the target sequence and multiple scrambled sequences displayed similar peak heights to
550 those in alginate-dsDNA. Importantly, there was a greater distinction between the
551 mixtures containing the target and those without for hydrogels containing the 2'-F
552 modification. Notably, spectra of mixtures without the target sequence displayed peak
553 heights similar to the ss 2'-F Oligo, while mixtures with the target sequence exhibited a
554 blue-shifted peak (shift to 270 nm) with similar maxima to the probe+target duplex.

555
556 The addition of a mismatched sequence to larger mixtures was also investigated (Figure
557 S14) and produced spectra that mimicked the alginate-dsDNA spectrum, though with
558 slightly elevated peak heights for both unmodified DNA and 2'-F Oligo (F-All_{DNA}). While
559 slight differences were observed in the CD spectra, the variability introduced by the
560 mixtures complicates definitive conclusions regarding the specificity of the hydrogel for
561 the target sequence. However, PCA effectively separated hydrogels according to the
562 presence of the target strand (Figure 6). Dimension 1 clearly delineated spectra
563 containing the target sequence from those without it, with greater separation observed for
564 fluorine-modified samples. This is likely due to the increased differences in peak heights
565 and greater shifts in CD peak maxima in samples containing the target sequence versus
566 those without it. In fact, variation in dimension 1 was mainly attributed to wavelengths 242
567 nm - 247 nm and 269 nm - 276 nm (positive and negative CD maxima), further supporting
568 these claims. Variation in dimension 2 was primarily attributed to wavelengths ranging
569 from 251 nm -265 nm (positive CD maxima for samples containing the target sequence).

570



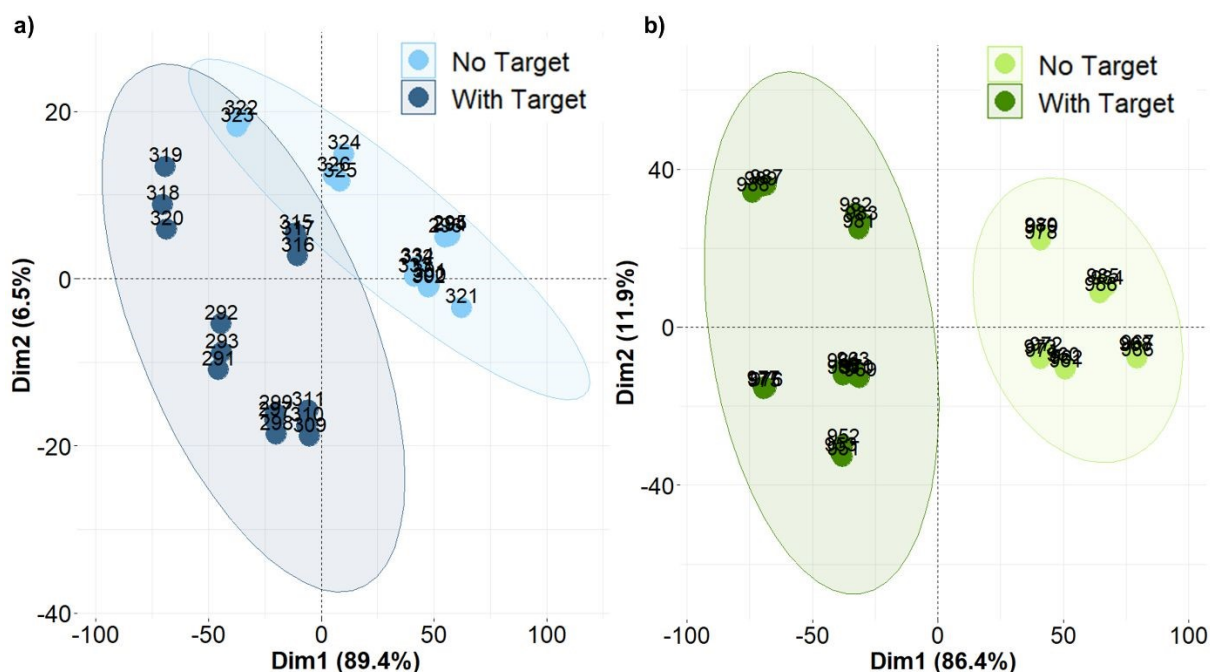


Figure 6. PCA score plot from **a)** DNA and **b)** 2'-F Oligo (F-All_{DNA}) specificity study samples, excluding samples with mismatch sequence. Samples with the mismatch sequence were excluded, as it was previously established that the mismatch could partially bind to the Probe strand and form a duplex. PCA data were truncated to focus only on wavelengths in the oligonucleotide region of the spectra (230 nm - 290 nm) and were not normalized, as relative peak heights of mixtures compared to standard duplexes are important markers for discrimination between sample types.

3.4.1 Temperature Melt (T_m) Analysis

Table 5. Averaged Temperature Melt Values for DNA and 2'-F Oligo Samples

Sample Contains	DNA T_m (°C)	2'-F Oligo T_m (°C)
DNA Target	70	81
Mismatch	51	53
Mismatch + DNA Target	74	83
Scrambled A	47	45
Scrambled A + DNA Target	69	78
Scrambled B	58	56
Scrambled B + DNA Target	76	81
Scrambled C	NA	52
Scrambled C + DNA Target	73	79
Scrambled B + Scrambled C	52	52
Scrambled B + Scrambled C + DNA Target	73	82
Scrambled A + Scrambled B + Scrambled C	56	NA
Scrambled A + Scrambled B + Scrambled C + DNA Target	73	84
Mismatch + Scrambled A	54	55
Mismatch + Scrambled A + DNA Target	72	83



Mismatch + Scrambled A + Scrambled B + Scrambled C	57	58
Mismatch + Scrambled A + Scrambled B + Scrambled C + DNA Target	74	83

582

583 All mixtures containing target sequences displayed higher T_m values than their
584 corresponding mixtures without the target (Table 3). The average difference in T_m values
585 for mixtures with and without the target strand was 19 °C, which increased to 28 °C for
586 fluorine-modified DNA. This suggests that the 2'-F Oligo (F-All_{DNA}) has stronger binding
587 to the DNA target sequence, resulting in greater T_m differences and improved specificity.
588 2'-F nucleobase modifications are known to increase duplex stability by enhancing base
589 stacking²⁸ and strengthening Watson-Crick base pairing²². In addition, 2'-F oligos offer
590 significantly greater environmental stability compared to DNA-based sensors.⁵⁵ While
591 DNA degrades over time⁵⁶, studies indicate that 2'-F oligos are resistant to nucleases with
592 enhanced stability,^{55, 57}, making them promising candidates for long-lasting biosensors.

593 3.4.2 Random Forest Classification

594 Random forest models were built using both CD spectra and temperature melt data, then
595 used to classify samples according to the presence of the target sequence. We achieved
596 high prediction accuracies when predicting classes of unknown (i.e., withheld) data from
597 the specificity studies. When only using CD data, we achieved a classification accuracy
598 of 77 % for unmodified DNA. When only using the temperature melt data, the accuracy
599 decreased to 60 %. However, when both datasets were combined using the average of
600 the replicates, classification accuracy reached 83 %. For the 2'-F Oligo (F-All_{DNA}), the
601 accuracy was 90% when using only CD data and 48% when using only temperature melt
602 data. When both datasets were combined, samples were correctly classified more than
603 95% of the time. These findings demonstrate that integrating CD spectra with temperature
604 melt data enhances classification accuracy, particularly when dealing with complex
605 mixtures containing similar sequences to those of the intended target. This is important,
606 as we clearly demonstrate that 2'-fluoro nucleobase modifications significantly increase
607 both sensitivity and target specificity without the need for amplification or complex and
608 expensive labelling techniques.

609 4. Conclusion

610 We synthesized a label-free, amplification-free, and immobilization-free short
611 oligonucleotide-based biosensor in which complement hybridization was detected and
612 recorded using CD spectroscopy. We increased the sensitivity and specificity of our
613 biosensor by adding a fluorine atom at the 2' position of the oligonucleotide sugar. The
614 changes in chirality due to conformational rearrangements could be observed in the CD
615 spectra as an increase in peak height and shifts in peak maxima. The alginate-oligo
616 hydrogels were synthesized using EDC/NHS coupling and CuAAC reactions. We first
617 confirmed the synthesis of the alginate-azide hydrogel using FTIR, where we observed
618 peaks attributed to the formation of an amide bond. Oligonucleotides were bound to the
619 alginate-azide via CuAAC, and the products were isolated by centrifugal filtering. CD
620 spectra were acquired to confirm the presence of DNA or RNA, and hybridization with the



621 complement was observed through increased ellipticity and blue-shifted long-wavelength
622 crossovers. Biosensors displayed great sensitivity with limits of detection of 2.9 nmol and
623 2.1 nmol for 2'F DNA- and RNA-based sensors, respectively, surpassing their unmodified
624 counterparts in the case of DNA. The 2'F modified oligo biosensor was also shown to be
625 more specific for its target complementary sequence than the unmodified version when
626 placed in mixtures with several non-complementary strands. Chemometric models
627 combining CD spectra with temperature melt data demonstrated higher classification
628 accuracies for fluorine-modified DNA (95%) than its unmodified counterpart (83%).
629 Although CD spectroscopy is not traditionally known to be a technique that can
630 discriminate between samples with similar composition, we have demonstrated that it is
631 possible to do so by pairing it with chemometrics. We have demonstrated that it is possible
632 to synthesize highly sensitive and specific biosensors by modifying nucleobases within
633 the DNA/RNA probe strand, and detecting hybridization without the need for traditional
634 complex approaches like amplification, labelling, or immobilization. Future work should
635 focus on improving discrimination between the target strand and strands containing
636 similar sequences with a few mismatches in more complex sample matrices.
637
638



639 REFERENCES

- 640 (1) Turner, A. P. Biosensors: sense and sensibility. *Chemical Society Reviews* **2013**, *42* (8),
641 3184-3196.
- 642 (2) Hua, Y.; Ma, J.; Li, D.; Wang, R. DNA-based biosensors for the biochemical analysis: A
643 review. *Biosensors* **2022**, *12* (3), 183.
- 644 (3) Bhalla, P.; Singh, N. Generalized Drude scattering rate from the memory function formalism:
645 an independent verification of the Sharapov-Carbotte result. *The European Physical Journal B*
646 **2016**, *89*, 1-8.
- 647 (4) Chen, J.-K.; Zhou, G.-Y.; Chang, C.-J.; Cheng, C.-C. Label-free detection of DNA
648 hybridization using nanopillar arrays based optical biosensor. *Sensors and Actuators B:*
649 *Chemical* **2014**, *194*, 10-18.
- 650 (5) Bush, J.; Hu, C.-H.; Veneziano, R. Mechanical properties of DNA hydrogels: Towards highly
651 programmable biomaterials. *Applied Sciences* **2021**, *11* (4), 1885.
- 652 (6) Hu, X.; Zhang, L.; Yan, L.; Tang, L. Recent advances in polysaccharide-based physical
653 hydrogels and their potential applications for biomedical and wastewater treatment.
654 *Macromolecular Bioscience* **2022**, *22* (9), 2200153.
- 655 (7) Orr, A.; Wilson, P.; Stotesbury, T. DNA-Crosslinked Alginate Hydrogels: Characterization,
656 Microparticle Development, and Applications in Forensic Science. *ACS Applied Polymer*
657 *Materials* **2022**, *5* (1), 583-592.
- 658 (8) Wang, Y.; Zhang, Y.; Zhang, Q.; Li, X.; Yan, Q.; Zhu, Y. Mechanical properties modulation
659 and biological applications of DNA hydrogels. *Advanced Sensor and Energy Materials* **2024**, *3*
660 (3), 100113.
- 661 (9) Gačanin, J.; Synatschke, C. V.; Weil, T. Biomedical applications of DNA-based hydrogels.
662 *Advanced Functional Materials* **2020**, *30* (4), 1906253.
- 663 (10) Jung, I. Y.; Lee, E. H.; Suh, A. Y.; Lee, S. J.; Lee, H. Oligonucleotide-based biosensors for
664 in vitro diagnostics and environmental hazard detection. *Analytical and Bioanalytical Chemistry*
665 **2016**, *408* (10), 2383-2406. DOI: 10.1007/s00216-015-9212-2.
- 666 (11) Toldrà, A.; Alcaraz, C.; Diogène, J.; O'Sullivan, C. K.; Campàs, M. Detection of *Ostreopsis*
667 cf. *ovata* in environmental samples using an electrochemical DNA-based biosensor. *Science of*
668 *the total environment* **2019**, *689*, 655-661.
- 669 (12) Jung, I. Y.; You, J. B.; Choi, B. R.; Kim, J. S.; Lee, H. K.; Jang, B.; Jeong, H. S.; Lee, K.;
670 Im, S. G.; Lee, H. A Highly Sensitive Molecular Detection Platform for Robust and Facile
671 Diagnosis of Middle East Respiratory Syndrome (MERS) Corona Virus. *Advanced Healthcare*
672 *Materials* **2016**, *5* (17), 2168-2173. DOI: <https://doi.org/10.1002/adhm.201600334>.
- 673 (13) Moitra, P.; Alafeef, M.; Dighe, K.; Frieman, M. B.; Pan, D. Selective naked-eye detection of
674 SARS-CoV-2 mediated by N gene targeted antisense oligonucleotide capped plasmonic
675 nanoparticles. *ACS nano* **2020**, *14* (6), 7617-7627.
- 676 (14) McGoldrick, L. K.; Halámek, J. Recent advances in noninvasive biosensors for forensics,
677 biometrics, and cybersecurity. *Sensors* **2020**, *20* (21), 5974.



- 678 (15) Hai, X.; Li, Y.; Zhu, C.; Song, W.; Cao, J.; Bi, S. DNA-based label-free electrochemical
679 biosensors: From principles to applications. *TrAC Trends in Analytical Chemistry* **2020**, *133*,
680 116098.
- 681 (16) Endo, T.; Kerman, K.; Nagatani, N.; Takamura, Y.; Tamiya, E. Label-free detection of
682 peptide nucleic acid– DNA hybridization using localized surface plasmon resonance based
683 optical biosensor. *Analytical Chemistry* **2005**, *77*(21), 6976-6984.
- 684 (17) Chen, Z.; Mao, K.; Xue, J.; Feng, R.; Zhang, K.; Su, J.; Du, W.; Ran, J.; Yang, C.; Yang, Z.;
685 et al. Development and application of DNA hydrogels in biosensing: Current status and future
686 implications. *Microchemical Journal* **2025**, *213*, 113664. DOI:
687 <https://doi.org/10.1016/j.microc.2025.113664>.
- 688 (18) Chen, Y.; Qian, C.; Liu, C.; Shen, H.; Wang, Z.; Ping, J.; Wu, J.; Chen, H. Nucleic acid
689 amplification free biosensors for pathogen detection. *Biosensors and Bioelectronics* **2020**, *153*,
690 112049.
- 691 (19) Sidstedt, M.; Rådström, P.; Hedman, J. PCR inhibition in qPCR, dPCR and MPS—
692 mechanisms and solutions. *Analytical and bioanalytical chemistry* **2020**, *412*(9), 2009-2023.
- 693 (20) Fazakerley, G.; Uesugi, S.; Izumi, A.; Ikehara, M.; Guschlbauer, W. A→ Z transition in the
694 synthetic hexanucleotide (dCdGfl) 3. *FEBS letters* **1985**, *182*(2), 365-369.
- 695 (21) Ikeda, H.; Fernandez, R.; Barchi Jr, J. J.; Huang, X.; Marquez, V. E.; Wilk, A. The effect of
696 two antipodal fluorine-induced sugar puckers on the conformation and stability of the Dickerson-
697 Drew dodecamer duplex [d (CGCGAATTCGCG)] 2. *Nucleic acids research* **1998**, *26*(9), 2237-
698 2244.
- 699 (22) Manoharan, M.; Akinc, A.; Pandey, R. K.; Qin, J.; Hadwiger, P.; John, M.; Mills, K.;
700 Charisse, K.; Maier, M. A.; Nechev, L. Unique gene-silencing and structural properties of
701 2'-fluoro-modified siRNAs. *Angewandte Chemie* **2011**, *123*(10), 2332-2336.
- 702 (23) Prakash, T. P. An overview of sugar-modified oligonucleotides for antisense therapeutics.
703 *Chemistry & biodiversity* **2011**, *8*(9), 1616-1641.
- 704 (24) Khvorova, A.; Watts, J. K. The chemical evolution of oligonucleotide therapies of clinical
705 utility. *Nature biotechnology* **2017**, *35*(3), 238-248.
- 706 (25) Heinemann, U.; Roske, Y. Symmetry in nucleic-acid double helices. *Symmetry* **2020**, *12*
707 (5), 737.
- 708 (26) Evich, M.; Spring-Connell, A. M.; Germann, M. W. Impact of modified ribose sugars on
709 nucleic acid conformation and function. *Heterocyclic Communications* **2017**, *23*(3), 155-165.
- 710 (27) Watts, J. K.; Choubdar, N.; Sadalpure, K.; Robert, F.; Wahba, A. S.; Pelletier, J.; Pinto, B.
711 M.; Damha, M. J. 2'-fluoro-4'-thioarabino-modified oligonucleotides: conformational switches
712 linked to siRNA activity. *Nucleic Acids Res* **2007**, *35*(5), 1441-1451. DOI: 10.1093/nar/gkl1153
713 From NLM.
- 714 (28) Guo, F.; Li, Q.; Zhou, C. Synthesis and biological applications of fluoro-modified nucleic
715 acids. *Organic & biomolecular chemistry* **2017**, *15*(45), 9552-9565. DOI: 10.1039/c7ob02094e.
- 716 (29) Patra, A.; Paolillo, M.; Charisse, K.; Manoharan, M.; Rozners, E.; Egli, M. 2'-Fluoro RNA
717 shows increased Watson-Crick H-bonding strength and stacking relative to RNA: evidence from



- 718 NMR and thermodynamic data. *Angew Chem Int Ed Engl* **2012**, *51* (47), 11863-11866. DOI:
719 10.1002/anie.201204946 From NLM.
- 720 (30) Lesnik, E. A.; Guinosso, C. J.; Kawasaki, A. M.; Sasmor, H.; Zounes, M.; Cummins, L. L.;
721 Ecker, D. J.; Cook, P. D.; Freier, S. M. Oligodeoxynucleotides containing 2'-O-modified
722 adenosine: synthesis and effects on stability of DNA: RNA duplexes. *Biochemistry* **1993**, *32*
723 (30), 7832-7838.
- 724 (31) Lee, K. Y.; Mooney, D. J. Alginate: Properties and biomedical applications. *Progress in*
725 *Polymer Science* **2012**, *37*(1), 106-126. DOI: 10.1016/j.progpolymsci.2011.06.003.
- 726 (32) Liparoti, S.; Speranza, V.; Marra, F. Alginate hydrogel: The influence of the hardening on
727 the rheological behaviour. *Journal of the Mechanical Behavior of Biomedical Materials* **2021**,
728 *116*, 104341.
- 729 (33) Guo, X.; Wang, Y.; Qin, Y.; Shen, P.; Peng, Q. Structures, properties and application of
730 alginic acid: A review. *International Journal of Biological Macromolecules* **2020**, *162*, 618-628.
- 731 (34) Kong, H. J.; Kaigler, D.; Kim, K.; Mooney, D. J. Controlling rigidity and degradation of
732 alginate hydrogels via molecular weight distribution. *Biomacromolecules* **2004**, *5*(5), 1720-
733 1727.
- 734 (35) Zhang, C.; Grossier, R.; Candoni, N.; Veessler, S. Preparation of alginate hydrogel
735 microparticles by gelation introducing cross-linkers using droplet-based microfluidics: a review
736 of methods. *Biomaterials Research* **2021**, *25*(1), 41.
- 737 (36) LeRoux, M. A.; Guilak, F.; Setton, L. A. Compressive and shear properties of alginate gel:
738 effects of sodium ions and alginate concentration. *Journal of Biomedical Materials Research: An*
739 *Official Journal of The Society for Biomaterials, The Japanese Society for Biomaterials, and The*
740 *Australian Society for Biomaterials and the Korean Society for Biomaterials* **1999**, *47*(1), 46-53.
- 741 (37) Ahmed, E. M. Hydrogel: Preparation, characterization, and applications: A review. *Journal*
742 *of advanced research* **2015**, *6*(2), 105-121.
- 743 (38) Jaganathan, H.; Kinsella, J. M.; Ivanisevic, A. Circular Dichroism Study of the Mechanism
744 of Formation of DNA Templated Nanowires. *Chemphyschem* **2008**, *9*(15), 2203-2206. DOI:
745 10.1002/cphc.200800509.
- 746 (39) Shi, P.; Zhao, N.; Coyne, J.; Wang, Y. DNA-templated synthesis of biomimetic cell wall for
747 nanoencapsulation and protection of mammalian cells. *Nat Commun* **2019**, *10*(1), 2223. DOI:
748 10.1038/s41467-019-10231-y From NLM Medline.
- 749 (40) Presolski, S. I.; Hong, V. P.; Finn, M. G. Copper-Catalyzed Azide-Alkyne Click Chemistry
750 for Bioconjugation. *Curr Protoc Chem Biol* **2011**, *3*(4), 153-162. DOI:
751 10.1002/9780470559277.ch110148 From NLM.
- 752 (41) Rahman, N.; Khan, S. Circular dichroism spectroscopy: A facile approach for quantitative
753 analysis of captopril and study of its degradation. *ACS omega* **2019**, *4*(2), 4252-4258.
- 754 (42) Santos-Cancel, M.; White, R. J. Collagen Membranes with Ribonuclease Inhibitors for
755 Long-Term Stability of Electrochemical Aptamer-Based Sensors Employing RNA. *Analytical*
756 *Chemistry* **2017**, *89*(10), 5598-5604. DOI: 10.1021/acs.analchem.7b00766.
- 757 (43) Gray, D. M.; Ratliff, R. L.; Vaughan, M. R. [19] Circular dichroism spectroscopy of DNA.
758 In *Methods in Enzymology*, Vol. 211; Academic Press, 1992; pp 389-406.



- 759 (44) Paul, P.; Suresh Kumar, G. Thionine Interaction to DNA: Comparative Spectroscopic
760 Studies on Double Stranded Versus Single Stranded DNA. *Journal of Fluorescence* **2012**, *22* (1),
761 71-80. DOI: 10.1007/s10895-011-0931-2.
- 762 (45) Hammill, M. The synthesis and in vitro evaluation of chemically modified siRNAs that
763 contain internal azobenzene derivative spacers for selective and tunable photocontrol of activity.
764 2017.
- 765 (46) Kypr, J.; Kejnovská, I.; Renčuk, D.; Vorlíčková, M. Circular dichroism and conformational
766 polymorphism of DNA. *Nucleic acids research* **2009**, *37* (6), 1713-1725.
- 767 (47) Arghavani, M. B.; SantaLucia, J.; Romano, L. J. Effect of mismatched complementary
768 strands and 5' -change in sequence context on the thermodynamics and structure of benzo [a]
769 pyrene-modified oligonucleotides. *Biochemistry* **1998**, *37* (23), 8575-8583.
- 770 (48) Kakiuchi, N.; Marck, C.; Rousseau, N.; Leng, M.; De Clerq, E.; Guschlbauer, W.
771 Polynucleotide helix geometry and stability. Spectroscopic, antigenic and interferon-inducing
772 properties of deoxyribose-, ribose-, or 2'-deoxy-2'-fluororibose-containing duplexes of
773 poly(inosinic acid) . poly(cytidylic acid). *Journal of Biological Chemistry* **1982**, *257* (4), 1924-
774 1928. DOI: [https://doi.org/10.1016/S0021-9258\(19\)68127-5](https://doi.org/10.1016/S0021-9258(19)68127-5).
- 775 (49) Islam, M. N.; Masud, M. K.; Haque, M. H.; Hossain, M. S. A.; Yamauchi, Y.; Nguyen, N.
776 T.; Shiddiky, M. J. RNA biomarkers: diagnostic and prognostic potentials and recent
777 developments of electrochemical biosensors. *Small Methods* **2017**, *1* (7), 1700131.
- 778 (50) Wang, J.; Hui, N. Electrochemical functionalization of polypyrrole nanowires for the
779 development of ultrasensitive biosensors for detecting microRNA. *Sensors and Actuators B:
780 Chemical* **2019**, *281*, 478-485.
- 781 (51) Bolourinezhad, M.; Rezayi, M.; Meshkat, Z.; Soleimanpour, S.; Mojjarrad, M.; Aghae-
782 Bakhtiari, S. H.; Taghdisi, S. M. Design of a rapid electrochemical biosensor based on
783 MXene/Pt/C nanocomposite and DNA/RNA hybridization for the detection of COVID-19.
784 *Talanta* **2023**, *265*, 124804.
- 785 (52) Fan, C.; Plaxco, K. W.; Heeger, A. J. Electrochemical interrogation of conformational
786 changes as a reagentless method for the sequence-specific detection of DNA. *Proceedings of the
787 National Academy of Sciences* **2003**, *100* (16), 9134-9137.
- 788 (53) Lu, X.; Dong, X.; Zhang, K.; Han, X.; Fang, X.; Zhang, Y. A gold nanorods-based
789 fluorescent biosensor for the detection of hepatitis B virus DNA based on fluorescence resonance
790 energy transfer. *Analyst (London)* **2013**, *138* (2), 642-665. DOI: 10.1039/c2an36099c.
- 791 (54) Hu, R.; Liu, T.; Zhang, X.-B.; Huan, S.-Y.; Wu, C.; Fu, T.; Tan, W. Multicolor Fluorescent
792 Biosensor for Multiplexed Detection of DNA. *Analytical Chemistry* **2014**, *86* (10), 5009-5016.
793 DOI: 10.1021/ac500618v.
- 794 (55) Sanroman-Iglesias, M.; Lawrie, C. H.; Liz-Marzan, L. M.; Grzelczak, M. The role of
795 chemically modified DNA in discrimination of single-point mutation through plasmon-based
796 colorimetric assays. *ACS Applied Nano Materials* **2018**, *1* (7), 3741-3746.
- 797 (56) Xue, C.; Huang, H.; Wang, L.; Liao, W.; Jiang, H.; Wu, Z.-S. Swelling of serum-stable
798 DNA nanoparticles upon target-induced conformational rearrangement of sensing probes for the
799 signal-on detection of cancer-related genes. *Analytical Chemistry* **2022**, *94* (6), 2749-2756.



800 (57) Lietard, J.; Abou Assi, H.; Gomez-Pinto, I.; González, C.; Somoza, M. M.; Damha, M. J.
801 Mapping the affinity landscape of Thrombin-binding aptamers on 2' F-ANA/DNA chimeric G-
802 Quadruplex microarrays. *Nucleic acids research* **2017**, *45* (4), 1619-1632.
803
804



805 ASSOCIATED CONTENT

806 **Author Contributions**

807 The manuscript was written through contributions of all authors. All authors have given approval to the final version of
808 the manuscript. ‡These authors contributed equally. (match statement to author names with a symbol)

809 **Funding Sources**

810 We are thankful for the funding support to conduct this research. This work was
811 supported by the Natural Sciences and Engineering Research Council of Canada
812 (NSERC) Discovery and Discovery Accelerator Supplement Grants (RGPIN-2020-
813 05816) awarded to TS and NSERC Discovery (RGPIN-2019-04692) awarded to JPD.
814 Author DL received the Ontario Tech University Student Training Assistantships in
815 Research (STAR) and is currently supported through The Graduate International Tuition
816 Scholarship (GITS). Author CE is currently supported through the NSERC CGS-D
817 program.

818 **Notes**

819 The authors declare no competing financial interest.

821 **ACKNOWLEDGMENT**

822 Thank you to Dr. Matthew Hammil for his help with the synthesis of the DNA and RNA
823 sequences.

824 **ABBREVIATIONS**

825 °C, Degrees Celsius; **CD**, Circular dichroism; **CuAAC**, Copper-(I) catalyzed azide-
826 alkyne cycloaddition; **ds**, double stranded; **EDC**, 1-ethyl-3-(3-dimethylaminopropyl)
827 carbodiimide hydrochloride; **FTIR**, Fourier Transform Infrared; **G'**, Storage Modulus; **G''**,
828 Loss Modulus; **LVE**, linear viscoelastic range; **NHS**, N-hydroxysuccinimide; **NIST**,
829 National Institute of Standards and Technology; **nm**, nanometers; **nM**, nanomole; **NMR**,
830 Nuclear magnetic resonance; **OD**, Optical Density; **SRM**, Standard reference materials;
831 **ss**, single stranded; **UV-Vis**, Ultraviolet-Visible

832
833
834



Data availability statement:

The data supporting this article have been included as part of the Supplementary Information. Supplementary information include additional spectroscopic and rheological characterization, a full list of sample names and additional PCAs.

